# Imbricated Beachrock Deposits Adjacent to the Java Trench, Indonesia: Influence of Tsunami and Storm Waves

**Ronald A Harris** ( rharris@byu.edu )
Brigham Young University https://orcid.org/0000-0001-5179-9877
**William Meservy**
Brigham Young University-Provo: Brigham Young University
**Hanif Sulaeman**
Brigham Young University-Provo: Brigham Young University
**Michael Bunds**
Utah Valley University
**Jeremy Andreini**
Utah Valley University
**Brierton Sharp**
Brigham Young University-Provo: Brigham Young University
**Bryce Barrett**
Oregon State University
**Jared Whitehead**
Brigham Young University-Provo: Brigham Young University
**Garrett Carver**
Brigham Young University-Provo: Brigham Young University
**Gelang Setiadi**
Universitas Pembangunan Nasional Veteran Yogyakarta
**Satrio Hapsoro**
Universitas Pembangunan Nasional Veteran Yogyakarta
**Carolus Prasetyadi**
Universitas Pembangunan Nasional Veteran Yogyakarta

---

**Research Article**

**Keywords:** Tsunami hazards, coastal boulder deposits, Java trench, mega-thrust earthquakes, tsunami modeling, Indonesia

**Posted Date:** March 24th, 2023

**DOI:** https://doi.org/10.21203/rs.3.rs-2720366/v1

# Abstract

We discovered several Imbricate Beachrock Deposits (IBD), one of which was observed to have formed during the tsunami caused by the 1994 7.8 Mw earthquake in East Java. Similar IBD were also found along the southern coastlines of central Java, Bali, Lombok, Sumba, Kisar, Leti and Nailaka Islands. The largest imbricated beachrock slabs are around $3m^3$. Most IBD are composed of thin, rectangular (2.5 x 1.7 x 0.4 m) slabs of calcareous beachrock dislodged from the intertidal platform during one or several powerful wave impactions. Ages of coral boulders incorporated into the IBD match with historical records of known tsunamigenic earthquakes offshore and candidate paleotsunami sand deposit ages onshore. To test for the influence of storms on the IBD we measured the positions of boulders over a 3-year period at one site by overlaying digital surface models created from UAV surveys. During the 3 years there were multiple uncommonly high wave events including two tropical cyclones. Around 113 individual beachrock slabs of the approximately 1220 slabs in the IBD were moved slightly or flipped within the deposit, but no conclusive evidence exists for addition or removal of beachrock slabs. The combination of data from various sources favors the hypothesis that the IBD are emplaced by tsunamis. If this is the case, then the IBD provide a durable record of previous tsunamis that should be incorporated into tsunami risk assessments for the highly populated coastlines of the eastern Sunda and Banda Arcs. We estimate from tsunami models that at least 6 million people inhabit likely inundation zones of worst-case scenario tsunamis generated by a Java Trench mega-thrust earthquake.


# 1.0 Problem

The Sunda Trench extends for 3200 km from offshore the Andaman Islands and Sumatra in the NW to Java and the Lesser Sunda Islands to the SE (Fig. 1). Historical and instrumental records document several mega-thrust earthquakes on the northern section of the Sunda Arc. A Mw = 9.2 mega-thrust event occurred on this section in 2004, which claimed around 230,000 lives mostly due to the mega-tsunami it produced (e.g., Lay et al. 2005). Although historical accounts from Dutch colonists in Indonesia reach back to 1584, there is scarce evidence that the SE section of the Sunda Arc, the Java Trench, has experienced mega-thrust earthquakes like those well documented in Sumatra during the past 439 years. Are these two parts of the Sunda Arc deforming in different ways? For example, does the Java Trench have a significant component of creep that explains the lack of instrumental earthquakes >Mw 7.8 or unequivocal mega-thrust earthquakes in historical records (Newcomb and McCann 1984)? Alternatively, is the Java Trench in a strain accumulation phase that exceeds the time window of historical accounts? If the latter is the case, then the seismic and tsunami risk is very high for one of the world's most densely populated coastal areas facing a loaded subduction zone.

If the Java Trench, which has a convergent rate of 70 mm/a (Nugroho et al. 2009), has been in an elastic strain accumulation phase for > 439 years. During this time the Java Trench could have accumulated at least 30 m of potential slip over a broad area that could produce a Mw 8.8–9.1 depending on possible rupture lengths of 500–1200 km, respectively. At the current state of seismic and tsunami readiness (Hall

et al. 2017), this event could claim as many or more lives than the 2004 megathrust earthquake of the northern Sunda Arc.

To test whether mega-thrust earthquakes and large tsunamis pre-date available historical accounts, or are not recognized as such, we investigated geological records of paleotsunami deposits along the southern coast of Java, Bali, and islands of the eastern Sunda Arc (Fig. 1). Candidate paleo-tsunami deposits include high-energy marine sand deposits in low-energy, terrestrial depositional environments, and distinct Imbricated Beachrock Deposits (IBD). This paper focuses on the origin of Indonesian IBD, and the possible influence of tsunamis related to past mega-thrust earthquakes. The possibility that the IBD are from storm waves is also investigated.

# 1.1 History of Tsunamigenic Earthquakes along the Java Trench

Some of the most densely populated coastal areas in Indonesia are adjacent to the Java Trench (Fig. 1). Historical records provide fussy data for only a few local tsunamis (Wichmann 1918 and 1922) that happened near Pacitan (Fig. 2) in 1840 and 1856, both with a MMI of VII (Harris and Major, 2016). The 1840 event shook for around two minutes. The lack of historical accounts that hint of mega-thrust earthquakes along the Java Trench may also be a function of lack of Dutch colonies along the coast or the slow-rupture style of earthquakes in the region. Early 18th century Dutch maps show the southern coast as" Parte Incognita" with virtually no Dutch settlements. The perceptivity of slow-rupture earthquakes may also account for the few historical accounts of strong shaking. Only two instrumental earthquakes > Mw 7.0 have happened along the subduction interface of the Java Trench in the past century (Figs. 1, 2). These events struck on 3 June 1994 (Mw 7.6 from Tsuji et al. 1995a, or Mw 7.9 from Hébert et al. 2012; Xia et al. 2021) and 17 July 2006 (M7.8 from Moore et al. 2011). Neither of these earthquakes were felt by most of the coastal inhabitants because they were slow slip "tsunami earthquakes" (Synolakis et al. 1995; Polet and Thio 2003; Fritz et al. 2007; Bilek and Engdahl 2007). Tsunami earthquakes produce uncommonly large waves relative to their recorded magnitudes (Tsuboi, 2000), and generate surface seismic waves with longer periods and slower velocities than typical subduction earthquakes.

Tsunamis from these two earthquakes had average wave heights of 5–7 m with maximum heights of up to 21 m in 2006 and 14 m in 1994 (Fig. 2). The tsunamis arrived at the coast within 30 minutes after the onset of the earthquake shaking, which limits the time for evacuation. Both tsunamis also reached the NW coast of Australia with run up heights of around 4 m (Nott, 2000; Prendergast and Brown 2011).

# 1.2 Paleo-tsunami evidence in the eastern Sunda Arc

Although historical records provide evidence of at least four earthquake-generated tsunamis hitting Java's southern coast, much of the corresponding geologic footprint of tsunamis is not well preserved. For example, evidence of Krakatoa's massive 1883 tsunami, which produced 37 m high waves and killed

over 36,000 people in West Java, is difficult to locate due to bioturbation, mass wasting, fish farming, resorts, industry, and agriculture (Paris et al., 2014). Java is the most densely populated, large island on Earth and is agronomically dominated from coast to coast; thus, there are very few areas along its southern coasts that have not historically and recently been disturbed.

Java is also one of the world's wettest islands located along a convergent plate boundary. Because of this, trenching efforts to prospect for candidate tsunami sand deposits are hampered by high levels of biotrubation and groundwater saturation. From our observations, most of the deposits from the 1994 and 2006 tsunamis are not preserved. These factors make it possible that lack of tsunami deposits is unrelated to tsunami size or recurrence. Recent attempts to locate paleotsunami sand sheets in swales of coastal plains of southern Java have yielded some success (Rizal et al., 2017; Sulaeman 2018). However, unequivocal diagnostic depositional features of tsunami sand layers are lacking (Dawson and Shi 2000; Goff et al. 2001; Scheffers and Kelletat 2003; Morton et al. 2007; Switzer and Jones 2008; Bourgeois 2009; Chagué-Goff et al., 2011).

The recognition of coastal boulder deposits along shorelines impacted by high-energy events, which include tsunamis, may provide a durable alternative to ephemeral tsunami sand deposits for recognizing the extent of tsunami impacted coastlines (e.g., Nott 2000; Nandasena et al. 2011a). The most likely processes that form these deposits are storm waves or tsunamis, but it is a challenge to unequivocally differentiate between the two (Nott 2003; Cox et al. 2020).

The surface of the Indian Ocean stretches virtually unimpeded from Antarctica to the southern shores of the Sunda Arc, a distance that facilitates generation of high waves that break along the southern coastal areas of the Sunda Arc. These large waves, especially at high spring tides, contribute to significant coastal erosion in the region (Hastuti et al. 2022). Storm waves have periods of 5–20 seconds (wavelengths of 100 to 200 meters) whereas tsunami wave trains are estimated to move at high velocities of 20–83 m/s across the continental shelf and 10–20 m/s near the shore, have periods from 10–120 minutes, and wavelengths around 500 km (e.g., Kato et al. 1991, 1995; Goto et al. 2009a and b).

The long duration and large amounts of water associated with tsunamis can have orders of magnitude more transport energy than the largest storm waves (Scheffers 2021). Although huge individual boulders and even boulder ridges are likely to have been emplaced and moved by wind waves (e.g. Goto et al., 2011; Cox et al., 2019), the construction of well-organized and imbricated beachrock slabs are rarely observed to form even from the largest known cyclones (Mastronuzzi and Sans`o 2000; Noormets et al. 2004; Nott 2004; Saintilan and Rogers 2005; Scheffers et al., 2005; Suanez et al., 2009; Scheffers and Kinis 2014). Nevertheless, some argue that imbrication of large rock slabs alone is not indicative of tsunamis alone (e.g., Etienne & Paris 2010; Goto et al. 2012), and is only one facet of interpreting the mechanism of IBD.

If large storms or cyclones form IBD, then the many beaches with joint-bounded beachrock in the intertidal zone throughout the world, especially those experiencing recurring category 4–5 cyclones, such as Florida would have IBD along its shores (Ginsburg 1953; Lau et al. 2015).

# 1.3 High Energy Storms in Indonesia?

The low rotational power of the Coriolis effect in Indonesia (< 10 degrees latitude) protects it from most cyclones. The rare cyclones that develop within 10 degrees of the equator spin away from Indonesia toward higher latitudes. Less than one percent of all the tropical cyclones from 1907 to 2017 in the Australian region crossed into Indonesian territory (Mulyana et al. 2018). In 2017, two category 1 tropical cyclones originated off the coast of Java but did not make landfall (Windupranata et al. 2019; Avia 2020). Sea wave heights from the storms increased from a 0.5 m normal wave height to an average of 2 m, with some waves locally reaching 3.2 m. However, much of the energy from these storms dissipates as the waves crash into the fringing reef at the edge of the shallow sub-tidal platform offshore. Notably, these storms did not form IBD. The only coastal boulder deposits documented from a Sunda Arc earthquake is associated with 2004 Indian Ocean Tsunami (Etienne et al., 2011; Szczucinski 2012).

# 1.4 Imbricate Beachrock Deposits (IBD)

IBD are a type of coastal boulder deposit where the 'boulders' consist mostly of overlapping, tabular (tile-like) beachrock slabs (Fig. 3). Most beachrock outcrops are found in the intertidal zone and consists of recently cemented, *in situ* beach sand. Layered beachrock outcrops are autochthonous to the beach and dip seaward (Fig. 3, 4) at around the same angle or slightly steeper than the slope of the beach (e.g., Russell, 1963; Davies and Kinsey, 1973). The majority of beachrock dated globally is 1000–5000 years old. However, these ages are skewed in an older direction due to lack of age data from modern beachrock (e.g., Scoffin 1993).

The most common occurrence of IBD are in tectonically active areas where beachrock slabs are carried landward until encountering an obstacle or backstop where they stack up (Goff et al. 2010; Schiffers and Kinis 2014). Cox et al. (2019) describe how this abrupt erosional step at the rear of the platform can block the transport of beachrock slabs causing a slab pile up (Figs. 3, 4). Commonly IBD form at around 25 m landward of excavated beachrock exposures. Some boulders make it over the backstop onto the coastal plain inland from the IBD ridge (Fig. 4). The presence of these boulders document large enough waves to not only inundate the coastal plain beyond the backstop but also to carry 2 m wide beachrock slabs there as well. These are processes not observed during storm wave activity in Indonesia or other tectonically active areas, such as Greece (e.g. Boulton and Whitworth, 2018).

The size and shape of IBD (Table 1) are characterized by a 3-axis system where the long axis (a) is commonly subparallel to the strike of the shoreline, the intermediate length axis (b) is parallel to the boulder transport direction, and the short axis (c) is the thickness of the slab (Nott 2000; Galvin 2003). These dimensions can be used to determine a flatness index 'Fb', where $Fb = (a + b)/2c$ (Cailleux and Tricart, 1959). A value of 1 is a square or round boulder, whereas higher values are tabular rock slabs like those found in most IBD (Table 1). We initially identified several sites along the southern coasts of the eastern Sunda Arc and Banda Arc where Google Earth images and attached photos hinted IBD existed. Ground surveys confirmed at least different IBD sites (Figs. 1, 2).

# 2.0 Methods

Within the IBD we document boulder position, size and movement using Unmanned Aerial Vehicles (UAVs) with 1 cm pixel resolution. The images were rasterized from point clouds made using surface-from-motion processing. The imagery was captured by a customized 24 Mp Sony A5100 camera with a 16- or 20-mm lens, and 20 Mp and 12.3 Mp DJI cameras. Cloud point georeferencing was co-registered with artificial and natural ground control points. These points were acquired by geodetic differential Global Navigation Satellite System receivers. The UAV surveys were enhanced by ground measurements of boulder size, orientation of dimension, elevation of highest boulders, minimum distance traveled and beach slope (Table 1). DEMs were differenced in ArcMAP using iterative closest point (e.g., CloudCompare) to construct Digital Surface Models (DSM). To detect boulder movement, we collected repeated measurements over a 3-year period at one site.

Radiocarbon age analyses were also conducted on several coral boulders imbricated with beachrock. Ages were determined by the Center for Applied Isotope Studies at the University of Georgia and were then calibrated using the online version of Calib 7.10 (Stuiver et al. 2019). Ages were calibrated (cal yr B.P.) to a 2s (95% probability) error range, where zero age is AD 1950. The non-marine (charcoal and root sheath) sample ages were calibrated using the SHCal13 curve (Hogg et al. 2013), and the marine sample (coral and shells) ages were calibrated using the Marine13 calibration curve (Reimer et al. 2013). Reservoir correction was determined by averaging $\Delta R$ data from nearby locations in northwestern Australia and western Java (Southon et al. 2002; O'Connor et al.; 2010, and Bowman 1985). Locations were chosen with consideration for proximity and ocean circulation. The value used for calibration was $\Delta R = 53 \pm 16$, with a lab error multiplier of 1.

Numerical models of potential inundation of a mega-thrust earthquake generated tsunami along the Java Trench were constructed using ComMIT (Titov et al., 2011). ComMIT is an interface developed for NCTR (NOAA's Center of Tsunami Research) that utilizes a "Method Of Splitting Tsunamis" (MOST). This program employs the shallow water equations for custom made fault plane solutions to model tsunamigenic earthquakes. The process is broken up into three steps/grids with each grid containing progressively higher resolution bathymetry and topography. These three steps include: earthquake, transoceanic propagation, and inundation of dry land. Bathymetry is from the ETOPO1 1 arc-minute gridded global relief model produced by the NOAA National Geophysical Data Center and has been interpolated from 60 arc seconds to 3 arc seconds. Higher-resolution bathymetry could improve the model. However, no higher resolution bathymetry has been released by the Indonesian government. Topography is from the CGIAR SRTM 90m version 4 digital elevation model produced by the CGIAR Consortium for Spatial Information.

Population within the inundation zone is calculated using two data sources: "World Pop" projected 2020 census distribution (www.worldpop.org.uk) and the 2015 "European Commission, Joint Research Centre" (JRC) census distribution (data.europa.eu). Through ArcMap GIS tools, data was clipped from inundated areas, and the sums were analyzed from both data sources.

# 3.0 Results

# 3.1 IBD in Java

We discovered seven supratidal IBD sites in Java (Fig. 2, Table 1). There are likely others either covered in sand or in parts of the coast we could not access. The most significant discovery was at Papuma (site J6, Fig. 1), a beach impacted by a tsunami from the 1994 7.9 Mw earthquake in east Java (Fig. 1). Although no tsunami height measurements were made at Papuma, nearby beaches recorded maximum tsunami heights from 11–14 m (Synolakis et al. 1995; Tsuji et al. 1995). By the time of our survey, sand deposits from the tsunami were scarce. However, residents and fishermen claim that the IBD at Papuma (Fig. 4a), and another site to the east at Pasir Putih (site J7), formed during the tsunami. Although the IBD were not mentioned during post-tsunami surveys (Maramai and Tinti 1997; Synolakis et al. 1995; Tsuji et al. 1995b) residents who witnessed the tsunami independently provided first-hand accounts of changes to the coastline that occurred including the formation of the IBD.

Papuma beach consists of outcrops of beachrock in the intertidal zone with layers that differ in resistance to erosion (Fig. 4). The outcrops show evidence of plucking of beachrock slabs from the intertidal zone, with pluck marks that match the size and shape of nearby detached slabs (Fig. 4). The minimum distance between sites of beachrock excavation and the IBD is around 25 meters up a beach slope of 5 degrees. At the base of the IBD the slope steepens abruptly to as much as 10–18 degrees (Fig. 4). Individual boulders in the Papuma IBD have consistent average strike directions within 6 degrees of the strike of the shoreline (Meservy (2017). After the tsunami, residents observed that some rock slabs were found on the beach road and further inland of the platform backstop.

Table 1
Location and characteristics of IBD.

| Place/Beach | Site | Latitude | Longitude | a-axis m | b-axis m | c-axis m | [a]Fb | Area $m^2$ | Elev m |
|---|---|---|---|---|---|---|---|---|---|
| **Java** | | | | | | | | | |
| Nampu | J1 | -8.210442 | 110.904169 | 2 | 1.2 | 0.3 | 5.3 | 2.4 | 3 |
| Klayar | J2 | -8.223617 | 110.947155 | 3.3 | 1.7 | 1.8 | 1.4 | 5.8 | 4 |
| Blosok | J3 | -8.234227 | 110.965912 | 3.4 | 2.2 | 0.3 | 9.3 | 9.6 | 4 |
| Pedenombo | J4 | -8.241134 | 110.983327 | 1.8 | 1.4 | 0.3 | 5.3 | 2.4 | 5 |
| Pidakan | J5 | -8.255659 | 111.238847 | 2.1 | 1.4 | 0.2 | 8.8 | 3.3 | 2 |
| Papuma | J6 | -8.435089 | 113.551749 | 2.4 | 1.9 | 0.3 | 7.2 | 4.7 | 4 |
| Pasir Putih | J7 | -8.561527 | 113.924558 | 0.8 | 0.7 | 0.5 | 1.5 | 0.6 | |
| **Bali** | | | | | | | | | |
| Pandawa | B1 | -8.843602 | 115.189514 | 2.6 | 1.8 | 0.3 | 7.3 | 4.6 | 3 |
| **Lombok** | | | | | | | | | |
| Are Guling | L1 | -8.913288 | 116.243961 | 2.5 | 1.3 | 0.3 | 6.3 | 3.2 | 4 |
| Putinyale | L3 | -8.909685 | 116.298494 | 2.2 | 1.8 | 0.4 | 5.0 | 4 | 4 |
| Payung | L4 | -8.917953 | 116.329526 | 3.6 | 2.8 | 0.6 | 5.3 | 10.3 | 4 |
| Kura-Kura | L5 | -8.919369 | 116.441725 | 3.4 | 2.3 | 0.3 | 9.5 | 7.9 | 5 |
| **Sumba** | | | | | | | | | |
| Maloba | S1 | -9.777156 | 119.651881 | 2.5 | 1.8 | 0.5 | 4.3 | 3.9 | 5 |
| **Kisar** | | | | | | | | | |
| SW coast | K1 | -8.050024 | 127.138544 | 1.8 | 1.2 | 0.6 | 2.5 | 2.2 | 8 |
| SW coast | K2 | -8.089577 | 127.146065 | | | | | | 20 |
| SW coast | K3 | -8.097237 | 127.145059 | | | | | | 19 |
| **Leti** | Lt1 | -8.213141 | 127.60159 | 3.2 | 1.6 | 0.6 | 4.0 | 5.1 | 4 |
| **Nailaka** | Bn1 | -4.535583 | 129.696464 | 2.7 | 1.5 | 0.4 | 5.3 | 4.1 | 3 |

a – Flatness Index (Fb) = (a + b) / 2c

Site J7 (Pasir Putih), which is in a nationally protected forest, translates to “White Sand Beach”. However, the 1994 tsunami removed all the sand from the beach and transformed it into one entirely covered by small (< 0.6 $m^2$), subrounded imbricated boulders and cobbles of that spill several meters over the platform backstop into the forest. The tsunami deposited what boulders were available offshore, which did not include exposed beachrock. This pattern of no IBD where there is little to no beachrock is common if not ubiquitous. Further west along the southern Java coast, in the Pacitan region, we discovered five additional IBD sites (Fig. 2, 4). Most of the beaches we investigated have a wide, flat platform that extends 150–200 meters seaward from the toe of the beach to the edge of barrier reef. The platforms are easily traversed during low tide because the large waves at these locations break offshore against the fringing reef. Large blocks of broken coral litter the outer edge of the platform, some of which have moved shoreward (Fig. 5).

According to Scheffers (2008) a shallow water platform setting makes it difficult for wind waves to move boulders and rock slabs due to loss of energy not only when the waves break at the fringing reef edge, but also as they travel across the width of the shallow platform. The boulders at each site, and source areas for the boulders, are mostly beachrock like what we observe at Papuma (Fig. 4). Some beaches have slabs of limestone from nearby bedrock outcrops and coral mixed in with the IBD. Well exposed areas of beachrock excavation show ramp-flat excavation plane geometries like those in imbricate thrust sheets (Fig. 3, 5a). Some slabs of beachrock have left scour marks in their wake that are traceable for > 100 m across the intertidal platform before deposition (Fig. 5b). Most exposed areas of beachrock in the intertidal zone are adjacent to IBD.

## 3.2 IBD East of Java

East of Java, IBD are found along the southern coastlines of Bali, Lombok, and Sumba of the eastern Sunda Arc, and along coastlines of the Banda Arc Islands of Kisar, Leti and Nailaka (Fig. 1). The Sunda Arc Islands face the Java Trench while the Banda Arc Islands face the Timor and Tanimbar Troughs, which is influenced by continental subduction (e.g., Harris, 2011). In Lombok IBD are up to 750 m long and 25 m wide at Kura-Kura Beach (site L4) in SE Lombok (Fig. 1, 4). Similar characteristics are found in these deposits as documented from the known tsunami deposit in Papuma.

## 3.3 Composition of IBD

The IBD we discovered mostly consist of slabs of dense, carbonate cemented sand and gravel of both clastic and biogenic origin (Fig. 7), which is characteristic of beachrock in general (e.g., Russell 1963; Bricker 1971; Milliman 1974; Vieira et al. 2007). Most beachrock is documented in mid-low latitude coastal regions and beaches with low tidal variation (Vousdoukas et al. 2007). Cementation of the beachrock mostly happens in the vadose zone during low tide when the sand deposits are exposed to the atmosphere. The lithification process is related to cementation of carbonate from fresh water (calcite) or sea water (aragonite) in the intertidal zone. Some studies show a strong correlation between beachrock formation and proximity to carbonate-rich shorelines. Most of the IBD sites in the eastern Sunda Arc are near carbonate bedrock. Although beachrock is a common feature of coastlines globally, ridges of

stacked or imbricated beachrock are rare except in tectonically active areas that are likely influenced by recurring tsunami.

Compositional exceptions to IBD are accumulations of boulders sourced from wave-cut cliffs. These varying-shaped boulders are also imbricated by high energy events (Fig. 7). IBD lacking beachrock are found at Nampu (site J1) and Klayar (site J2) in Java and Payung (L1) in Lombok (Fig. 2).

# 3.4 Size and orientation of IBD

Evidence of rapid undercutting and recent bedrock cliff failure and retreat is visible throughout much of southern coastlines of Java, Bali, Lombok, and the lesser Sunda Islands. Typically, when a coastal cliff collapses, or a landslide occurs near the coast, rocks from onshore are initially distributed randomly along the coastal bench. Large waves can break up some of these boulders and stack them in with beachrock slabs (Fig. 7).

In contrast, beachrock from the intertidal zone of the seafloor stacks up in a different way to produce IBD. *In situ* beach rock is constantly being attacked by storm waves causing differential erosion of some layers that introduce instabilities, such as overhangs that cause beachrock to break into allochthonous slabs (Fig. 6). Large waves transport most slabs from their source in the intertidal zone to near the maximum high tide mark to form IBD. Nearly all the stacked slabs of IBD are platy with average long a-axes of 2.8 m, intermediate axes (b-axis) of 1.8 m and thicknesses (c-axis) of 40 cm. Volumes of the largest boulders are 3–4 cubic m (Table 1). In general, the largest rock slabs are around the same size, with exceptions found at sites J4 and L4 (Table 1).

Most IBD have a preferred strike orientation of the a-b plane, which is sub-parallel to the strike of the shoreline within 2–10 degrees (Meservy 2017). All the beach rock slab accumulations have similar, right-skewed distributions with between 0.5-1.0 cubic meters in volume. Of the largest boulders, none are much greater than 3 cubic meters. Whether this size limit is a function of wave height or speed, or from the size of the boulders available is unknown (Benner et al 2010). Other studies demonstrate how boulder sizes do not correlate well with known wave speeds that deposited them (Etienne et al., 2011). More important are the sizes of the boulders available for the wave to entrain (Scheffers 2021). Nott (2003) notes that during the 1998 Sissano tsunami in Papua New Guinea a concrete slab with a- b- and c-axes of 3.15, 1.22 and 0.23, respectively, moved 400 meters inland from flow depths of 5 m. This depth is less than those inferred for Papuma.

# 3.5 Uncommon storm wave height experiment

IBD provide conditions for conducting experiments to test the contribution of storm waves in forming or shaping IBD (Oak 1984, Lorang 2002 Goto et al. 2007, Goto et al. 2009b, Benner et al. 2010; Goto et al. 2010a, Goto et al. 2010b, Etienne and Paris 2010, Goto et al. 2011; Schneider et al. 2019). Between 1983 and 2016 there have been 5 high wave events with an average of 4.7 m swells and periods of 18 – 10 seconds (Surfline.com) along the southern coastlines of eastern Sunda Arc islands.

To measure possible boulder movement during these storms we constructed UAV-assisted digital surface models (DSMs) with a high degree of boulder registration through time at Pedenombo beach (Fig. 8). This beach consists of 3 platforms. The lowest is the current wave cut platform forming the intertidal zone. The second is 3 m above sea level and likely represents a wind wave terrace. This platform hosts the IBD, which stack up against the shoreward edge of platform 3. The third platform could be an uplifted Holocene coral terrace or a slightly subsided 5e sea level high-stand terrace formed at approximately 120 ka.

High resolution UAV data were collected during four separate missions between 2016 and 2019. The first pre- and post-storm measurements were taken on 7/30–31/2016 and 8/2/2016, which was immediately before and after a 4.2 m swell that struck the beach during a + 2.5 m spring high tide (Surfline.com). The third set of drone images were taken on 7/12/2017 after an epoch of 342 days. The fourth set was taken 6/20/2019 after an epoch of 708 days. During this nearly two year period the beach was impacted by waves from two offshore tropical cyclones.

# 3.6 Discussion of DSM Overlays at Pedenombo

Image (a) is an orthophoto documenting the initial positions of IBD slabs 1 day before an uncommon storm wave event (Fig. 9a). Additionally, 21 limestone boulders < 0.5 m in diameter were marked, manually placed, and surveyed seaward of the IBD. See small open circles in Fig. 9b for original positions of hand placed boulders.

Image (b) is an overlay of DSMs from before and after the 6.7 m high wave event on 7/30–31/2016 (Fig. 9b). The image documents the initial and final positions of manually placed boulders and pre-existing beachrock slabs of the IBD (Fig. 11b). After the storm, we located all but two of the boulders and resurveyed their positions. Green circles show pre- and red triangles show post-storm locations. Lines on the image connect initial and final boulder positions and reveal that all manually placed boulders moved, if only 10 cm. Most boulders moved laterally along the shoreline, even off the image from 2–45 m. Five placed boulders were added to the front of the IBD, but none moved onto the IBD. At least 8 pre-existing beachrock slabs of the IBD moved < 2 m as indicated by the proximity of slab excavation and addition marks. The mirror image of some of these marks indicate slabs flipping about their a-axes.

Image (c) is an overlay of DSMs of the post-storm 2016 and 2017 UAV surveys. During this time waves from 2.2 m to 2.6 m were recorded on June 23, 2017 (Avia 2020). At least 19 IBD slabs moved < 2 m based on matching of green and nearby red shapes (Fig. 9c). The mirror image of some of these shapes indicate slab flipping about the a-axis as in Fig. 9b. At least 8 other slabs circled in green have ambiguous sources. These slabs may have been added to the IBD by storm waves (not likely based on other observations) or their original position is eroded or filled in by storm deposited sand, gravel, and cobbles. Changes in sand volume is detected at ten localized zones on the beach with an average volume change of approximately 65 $m^2$.

Image (d) is an overlay of DSM (c) and (d), which records the effects of some of the most energetic waves over the most time (two offshore tropical cyclones). During this time, overlapping category 1 cyclones Cempaka and Dahlia brushed by Java increasing wave heights from 1.8 m to 3.2 m (Windupranata et al. 2019; Avia 2020). Cempaka, which nearly made landfall in the Pedenombo beach area, affected 13 coastal communities in the Pacitan area. In total there were 41 deaths, 20,000 people evacuated, and around US$83.6 million in damages (Badan Nasional Penanggulangan Bencana). Although the final overlay is messy due to clastic sediment redistribution, it reveals that around 113 individual beachrock slabs moved slightly or flipped of the approximately 1220 slabs in the IBD. One boulder in the lower left corner of image (c) disappears in image (d). However, *there is no conclusive evidence of boulder addition or removal.* UAV-based post-tsunami surveys of the 2004 Indian Ocean Tsunami also found that no boulders were added to or removed from the tsunami formed IBD by monsoonal storms (Etienne et al. 2011). These results provide limits for Indonesian storm waves to move boulders and strongly support an interpretation that the IBD are primarily formed by tsunamis. However, it is important to recognize the role storm waves play in eroding beachrock in the intertidal zone into detached slabs that can be transported later by tsunami waves.

# 3.7 Radiocarbon analyses

Another way to test the relative contribution of storm versus tsunami waves in forming IBD is age analysis of coral interlayered with the beachrock slabs. These ages likely differ depending on whether coral boulders were emplaced by storms or tsunamis. Tsunami ages may cluster around the time of known historical or paleo-tsunami event whereas storm wave deposits could have a much broader age distribution since coral boulders could be added yearly. Dating IBD is problematic due to the likelihood of mixing offshore siliciclastic and bioclastic material of various ages (e.g., Mastronuzzi et al. 2000; Ishizawa et al. 2020).

Our reconnaissance age analysis of several coral boulders yielded reliable ages at 5 sites (Table 2). Although there is some scatter, most ages correspond closely with known historical tsunamis and candidate paleo-tsunamis in the eastern Sunda Arc (Sulaeman, 2018). Only six tsunamis affecting eastern Sunda Arc islands are recorded in historical accounts dating back to 1584 (Harris and Major 2016). Lack of possible events reduces the likelihood of coral boulder ages coinciding with known and inferred tsunamis by chance (Table 2). For example, the 1861 AD age of coral boulders in IBD near Pacitan is concordant with the 1859 Pacitan tsunami (Harris and Major 2016). The 1692 age of another boulder coincides with one of the largest earthquakes to strike Java documented in historical accounts. This event was felt widely throughout the region with a maximum MMI of X, had at least 13 months of aftershocks, and a tsunami of unknown extent (Harris and Major 2016). The 1474 AD age correlates with a 400–600 years BP OSL age of a candidate tsunami sand deposit at 1 meter depth in Bali (Sulaeman 2018). Similar high-energy sands with marine debris occur onshore at around the same depth throughout the southern coastal plains of the eastern Sunda Arc.

The wide spectrum of ages for the imbricate coral boulders we sampled across the five, widely spread beaches may result from many factors, which is not uncommon for coastal boulder accumulations (e.g.,

Vousdoukas et al., 2007). The age ranges may indicate that the IBDs have amassed over a series of events (Nott 1997 and 2004). Notwithstanding these issues, we point out that it is highly unlikely that most boulder ages are concordant with the limited number of events reported in historical records and the two proposed paleo-tsunami events in region. In fact, only two ages that do not correlate are those of 500–700 AD (Table 2). If these boulder ages correspond to a tsunami they are consistent with a ~ 500 year recurrence interval of mega-thrust earthquakes.

Table 2
Radiocarbon chronology of shells and coral boulders found wedged within five IBD in Java.

| Location | Sample Type | Calibrate Calendar Age | 95% Confidence | Possible Event |
|---|---|---|---|---|
| Binuangeun West Java | shell | 1053 AD | 990–1153 AD | 1200 – 800 AD Java Trench** |
| | shell | 991 AD | 908–1050 AD | 1200 – 800 AD Java Trench** |
| | coral boulder | 989 AD | 907–1049 AD | 1200 – 800 AD Java Trench** |
| | shell | 905 AD | 806–994 AD | 1200 – 800 AD Java Trench** |
| | Coral boulder | 663 AD | 596–724 AD | ? |
| Blosok-C Site J3 | coral boulder | 1861 AD | 1810–1880 AD | 1859 AD Pacitan |
| Blosok-B Site J3 | coral boulder | 1692 AD | 1640–1720 AD | 1699 AD Java |
| Blosok-A Site J3 | coral boulder | 551 AD | 500–580 AD | ? |
| Pidakan Site J5 | coral boulder | 1474 AD | 1440–1510 AD | 1400–1600 AD Java Trench** |
| Pedenombo Site J4 | Shell on boulder | 1177 AD | 1080–1220 AD | 1200 – 800 AD Java Trench** |
| Kisar 1* Site K1 | coral boulder | 1903 AD | 1898–1908 AD | 1896 AD Timor |
| Kisar 2* Site K2 | coral boulder | 1904 AD | 1897–1909 AD | 1896 AD Timor |
| * Boulder deposit on coral terrace, Major et al. (2013) ** Sulaeman (2018) *** | | | | |

The discovery of several tsunami related IBD along a 1200 km section of the south coastal regions of the eastern Sunda Arc (Sulaeman 2018) that are likely emplaced by tsunamis indicates that this region is as

susceptible to recurring mega-thrust earthquakes and large tsunamis as the western Sunda Arc (Sumatra). Candidate paleo-tsunami sand deposits discovered throughout the eastern Sunda Arc also attest to at least two large, multi-island tsunamis at around 1000 and 1500 AD (Sulaeman 2018). These findings are consistent with ages for some of the shells and coral boulders incorporated into the IBD of the Sunda Arc and NW Australia. We also found relatively young boulders deposited up to 20 meters above sea level on the 125 ka uplifted coral terrace in Kisar (Major et al. 2013). These ages are concordant with the 1896 earthquake and tsunami in Timor, which is the only major earthquake from the Timor region found in over 400 years of historical records (Harris and Major 2016).

# 3.8 NW Australia IBD from Java Trench Earthquakes?

IBD and large boulders at elevations up to 20 m along the 2500 km of coastline of NW Australia document huge waves impacting the coast before historical times (Nott and Bryant 2003; Goff and Chague-Goff 2014). Imbricated boulder ridges, like those we discovered along the southern coasts of the eastern Sunda Arc islands, are documented up to 6 m elevation. The largest boulder measured at the Australia IBD has an a-axis of 5 m, but the average boulder sizes are a = 3.0, b = 2.1, c = 0.7 m (Nott, 2004). Shells at the back of the ridge have radiocarbon chronologies dating around the mid to late 19th century, a period of heavy seismicity near Pacitan (Harris and Major 2016). Other ages roughly align with those of pre-historic tsunamis (Table 2).

Tsunamis that have impacted NW Australia during the last century were generated by the 1977 Sumba earthquake (Mw 8.3, Pradjoko et al 2015), and the 1994 (Mw 7.8) and 2006 (Mw 7.7) Java Trench earthquakes (Burbridge et al 2009). Runup heights in NW Australia from the 1977 and 1994 tsunamis were around 4 m (Nott and Bryant 2003). The 1994 tsunami transported coral boulders and marine fauna over 1000 m inland. The 2006 tsunami, which was further north on the Java Trench, had a flow depth of 1–2 m, maximum runup of 8 m, and inundated around 100–200 m inland (Prendergast and Brown 2011). None of the tsunamis formed new or noticeably modified existing IBD.

The NW Australian IBD at Exmouth consist mostly of beachrock like those we discovered in the eastern Sunda Arc. The fact that the 1994 Java Trench tsunami formed an IBD along the Java coast, but not in Australia may indicate that the Australia deposits require larger tsunamis from mega-thrust earthquake events. According to the age analysis of the boulders in the Exmouth IBD, a tsunami of this scale happens over time intervals of 400 to 500 years (Nott 2004), which is consistent with age distributions in the eastern Sunda ARC (Table 2). The age results from Australia and eastern Sunda Arc also argue strongly against IBD being formed by cyclones, which happen on a much more regular basis.

To test the potential of cyclones forming the NW Australia IBD, Nott (2004) conducted pre- and post-cyclone visual surveys. One of the mega-storms was TC Vance, which is the most intense category 5 cyclone ever recorded to cross Australian shores. Surveys were also taken after 3 other category 5 cyclones. These surveys found no evidence of IBD development even in areas where abundant loose boulders were available. Nott (2004) also claims that existing IBD were not disturbed by the mega-storms and no new beachrock slabs were added or removed. It is possible that IBD from the Indonesian locations

described in this paper and the ones at Exmouth, Australia may be emplaced by tsunamis from the same earthquakes with those of Australia only recording megathrust events on the Java Trench.

## 3.8 Tsunami modelling and inundation maps

If IBD in the eastern Sunda Arc and northern Australia record mega-thrust earthquake-caused tsunamis on the Java Trench, most of which have no historic precedent, then tsunami hazards risk assessments should consider the likelihood and impact of these events. To investigate this impact, we constructed tsunami models for two earthquake scenarios along the Java Trench, both of which could potentially form IBD simultaneously along the south coast of the eastern Sunda Arc islands and in NW Australia. We include estimates of the number of people currently inhabiting the areas of inundation in the models.

Model 1 is for an earthquake that fills the seismic gap between the 1994 and 2006 subduction interface earthquakes on the Java trench south of Java (Figs. 1 and 10). This gap could have ruptured to produce the 1859 and 1699 earthquakes and tsunamis noted in the Pacitan area where (Harris and Major 2016). The slip distribution from the 2011 East Japan earthquake is used to model an Mw = 8.4 earthquake on the subduction interface between the 1994 and 2006 tsunamigenic earthquakes. This location is also near where most of the IBD in Java are found (Fig. 12).

Model 2 (Fig. 11) is a worst-case scenario Mw = 9.0 mega-thrust earthquake that ruptures the seismic gap along the entire Java Trench. The amount of slip in this model is based on the sudden release of around 28 m of elastic strain or tectonic loading that has already accumulated on the 1200 m length Java Trench during the past 478 years (Harris and Major 2016). The result is at least a Mw 9.0 mega-thrust earthquake and associated tsunami like the December 2004 or the March 2011 East Japan mega-thrust events. The transoceanic propagation of this event (Fig. 12) shows the highest waves striking the western most tip of Australia where most of the IBD reported from this region are observed Nott (2000).

# 4.0 Discussion

Whether the Java Trench can generate mega-thrust earthquakes (> Mw 8.0) is still unknown. However, recent studies of seismic coupling (Hanifa et al 2014; Koulali et al 2018; Gunawan and Widiyantoro 2019) indicate that two large sections of the Java Trench are accumulating elastic strain and are not in a state of creep, as suggested by others (e.g, Newcomb and McCann 1987). IBD decorating the southern coastlines of multiple eastern Sunda Arc islands have similarities to those in NW Australia, such as the average size of the largest slabs, slab vs beach strike, composition, age, and clear excavations or dislodgements seaward from the IBD. Interpreting the processes involved in IBD formation is helped by a known tsunami emplaced IBD at Papuma. Many of the IBD we discovered at other locations are like those at Papuma, although some sites have much larger boulders. The size of beachrock slabs may depend more on joint spacing, pre-tsunami storm wave processing, or fragmentation during transport (Oetjen et al. 2021).

As revealed by DSM overlays, small (< 1.0 $m^2$) boulders we placed beachward of the IBD mostly moved eastward parallel to the longshore drift with some stopping at the toe of the IBD. Over the 3 year period we tracked the IBD boulders around 10% detectably moved. Consistent with observations by others (Nott 2003; Scheffers and Kinis 2014), no boulders were excavated from beachrock outcrops and added to the IBD by storm waves. Also, as in other examples, the uncommon storms that impacted the IBD during the 3 year epoch, which are the largest storms documented along the Sunda Arc coast (Windupranata et al., 2019), did not form IBD. If storms form IBD there should be multiple deposits associated with them in areas with beachrock that are battered regularly by cyclones, like NW Australia. Coral boulders caught up in storm-formed boulder deposit should have a wide range of ages.

Ages of coral boulders in IBD correspond to known historical, and inferred paleo-tsunami events that are separated by 100's of years. Ages from similar boulder deposits in Australia and the Sunda Arc also show a 400–600-year periodicity.

Scheffers (2004) concludes that boulder deposits from tsunamis are more likely to form ordered imbricate stacks of beach boulders due to the length of time tsunami waves inundate, versus the disarray of most boulders emplaced by storm waves. Again, this interpretation is consistent with the lack of documented boulder ridges in places impacted by gigantic storms, such as the NW coast of Australia (Nott, 2000). However, our results show that storm waves play an important role in first eroding beachrock into slabs completely or partially detached from outcrops in the intertidal region. In addition, matching boulder movements at Pedenombo indicates that storm waves modify existing IBD by flipping, and possibly sliding boulders short distances. At many beaches the most shoreward part of beachrock outcrops is undercut by wave action where the beachrock layers dip steeper than the beach slope angle. The overhangs that result commonly have rounded boulders (< 0.5 diameter) wedged into them likely from backwash (Figs. 3, 4). These wedged boulders exert an upward force on the overhangs and in some cases cause them to split off. These examples document how storm and tsunami wave action combine forces to form and shape IBD.

# 5.0 Conclusion

We claim that IBD are primarily deposited by tsunamis, based on direct observations of 1994 tsunami formed IBD at Papuma, the occurrence of long imbrication ridges of large boulders only adjacent to areas where beachrock was plucked from intertidal zones, the clustering age ranges of the boulders with paleo and historical events, lack of evidence for storm produced IBD (even during the largest storms known), and several IBD in tectonically active areas where no large storms happen, as in Indonesia. The existence of the IBD, especially in densely populated coastal areas as Java, Bali, and the Lesser Sunda Islands, are natural 'warning stones' of where tsunamis have likely inundated coastal areas in the past and as such must be incorporated into tsunami hazard risk reduction strategies. Tsunami models of a worst-case scenario Mw = 9.0 mega-thrust earthquake show that over 6 million people inhabit areas that would be inundated by such a tsunami. The locations of IBD certainly should be considered at high risk. However, it should also be noted that the processes that form IBD are not ubiquitous, but rather require unique

conditions, such as the formation of beachrock in the intertidal zone, storm wave processing of outcrops, and coastal geomorphology for the IBD to form and persist. Our tsunami models plainly show that areas without IBD are just as susceptible to tsunami hazards.

# Declarations

The authors have no relevant financial or non-financial interests to disclose.

All authors contributed to the study conception, design, material preparation, data collection and analysis. The first draft of the manuscript was written by William Meservy and all authors commented on previous versions of the manuscript. All authors read and approved the final manuscript.

**Acknowledgements**:

Funding for this research was generously provided through grants from Geoscientists Without Borders, which is affiliated with the Society of Exploration Geophysicists (SEG). Additional funds were provided by In Harm's Way non-profit organization (inharmswayhelp.com), Utah Valley University (UVU), and Brigham Young University (BYU). We thank Universitas Pembangunan Nasional (UPN Jogjakarta) who sponsors our research in Indonesia. We owe a special debt of gratitude to Eko Yulianto and Purna Putra from LIPI for collaboration in paleotsunami research in Indonesia. We express appreciation for logistic assistance from the BPBD and governor's offices of Pacitan, Mataram, Waingapu, Leti and Ambon. We are grateful for the logistical coordination help of Deborah Harris. We appreciate the many students from UPN, UVU and BYU, and both foreign and local volunteers who helped throughout the project.

# References

1. Avia L (2020) A Comparative Analysis of the Wind and Significant Wave Height on the Extreme Weather Events (TC Cempaka and TC Dahlia) in the Southern Sea of Java, Indonesia. IOP Conference Series: Earth and Environmental Science, IOP Publishing 572.1
2. Benner R, Browne T, Bruckner H, Kelletat D, Scheffers A (2010) Boulder transport by waves: progress in physical modelling. Zeitschrift fu¨r Geomorphologie, Supplementary Issues pp 127–146
3. Bilek S, Engdahl E (2007) Rupture characterization and aftershock relocations for the 1994 and 2006 tsunami earthquakes in the Java subduction zone. Geophysical Research Letters 34:20
4. Boulton S and Whitworth M (2018) Block and boulder accumulations on the southern coast of Crete (Greece): evidence for the 365 CE tsunami in the Eastern Mediterranean. Geological Society London, Spec. Pub., 456.1:105-125
5. Bourgeois J, Bernard E, Robinson A (2009) Geologic effects and records of tsunamis. The Sea 15:53-91
6. Bowman G (1985) Oceanic reservoir correction for marine radiocarbon dates from northwestern Australia. Australian Archaeology 20.1:58-67

7. Bricker, O (1971) Introduction: meteoric-water cementation. In: Bricker O (ed) Carbonate Cements. Johns Hopkins Press, Baltimore, pp. 121
8. Burbidge D, Cummins P, Mleczko R, Thio H (2009) A probabilistic tsunami hazard assessment for Western Australia. Tsunami Science Four Years after the 2004 Indian Ocean Tsunami: Part I: Modelling and Hazard Assessment.:2059-88.
9. Chagué-Goff C, et al (2011) Expanding the proxy toolkit to help identify past events—lessons from the 2004 Indian Ocean Tsunami and the 2009 South Pacific Tsunami. Earth-Science Reviews 107.1-2:107-122
10. Cox R, o'Boyle L, Cytrynbaum J (2019) Imbricated coastal boulder deposits are formed by storm waves, and can preserve a long-term storminess record. Scientific Reports 9.1:1-12
11. Cox R, Ardhuin F, Dias F, et al (2020) Systematic review shows that work done by storm waves can be misinterpreted as tsunami-related because commonly used hydrodynamic equations are flawed. Frontiers in Marine Science 7:4
12. Dawson A, Shi S (2000) Tsunami deposits. Pure and Applied Geophysics 157:875-897
13. Engel M, May S (2012) Bonaire's boulder fields revisited: evidence for Holocene tsunami impact on the Leeward Antilles. Quaternary Science Reviews 54:126-141
14. Etienne S, Paris R (2010) Boulder accumulations related to storms on the south coast of the Reykjanes Peninsula (Iceland). Geomorphology 114.1-2:55-70
15. Etienne S, Buckley M, Paris R, et al (2011) The use of boulders for characterizing past tsunamis: Lessons from the 2004 Indian ocean and 2009 South Pacific tsunamis. Earth-Science Reviews 107.1-2:76–90
16. Fritz H, Kongko W, Moore A, et al (2007) Extreme runup from the 17 July 2006 Java tsunami. Geophysical Research Letters 34.12
17. Ginsburg R (1953) Beachrock in South Florida. J of Sedimentary Research 23.2:85-92
18. Goff J, Chague-Goff C (2014) The Australian tsunami database: a review. Progress in Physical Geography 38.2:218-240
19. Goff J, Chagué-Goff C, Nichol S (2001) Palaeotsunami deposits: a New Zealand perspective. Sedimentary Geology 143.1-2:1-6
20. Goff J, et al (2010) Testing the hypothesis for tsunami boulder deposition from suspension. Marine Geology 277.1-4:73-77
21. Goto K, et al (2007). Distribution, origin and transport process of boulders deposited by the 2004 Indian Ocean tsunami at Pakarang Cape, Thailand. Sedimentary Geology 202.4:821-837
22. Goto K, Okada K, Imamura, F (2009a) Characteristics and hydrodynamics of boulders transported by storm waves at Kudaka Island, Japan. Marine Geology 262.1-4:14-24
23. Goto K, Okada K, Imamura, F (2009b) Importance of the Initial Waveform and Coastal Profile for Tsunami Transport of Boulders. Polish J of Environmental Studies 18.1

24. Goto K, Okada K, Imamura F (2010a) Discrimination of boulders deposited by tsunamis and storm waves at Ishigaki Island, Japan. Marine Geology 269.1-2:34-45
25. Goto K, Okada K, Imamura F (2010b) Numerical analysis of boulder transport by the 2004 Indian Ocean tsunami at Pakarang Cape, Thailand. Marine Geology 268.1-4:97-105
26. Goto K, Miyagib K, Kawanac T, Takahashia J, Imamuraa, F. (2011) Emplacement and movement of boulders by known storm waves — Field evidence from the Okinawa Islands, Japan. Marine Geology, 283.1-4: 6-78
27. Goto, K et al (2012) Sedimentary processes associated with sand and boulder deposits formed by the 2011 Tohoku-oki tsunami at Sabusawa Island, Japan. Sedimentary Geology 282:188-198
28. Gunawan E and Widiyantoro S (2019) Active tectonic deformation in Java, Indonesia inferred from a GPS-derived strain rate. J of Geodynamics 123:49-54
29. Hall S, Pettersson J, Meservy W, Harris R, Agustinawati D, Olson J, McFarlane A (2017) Awareness of tsunami natural warning signs and intended evacuation behaviors in Java, Indonesia. Natural hazards 89.1:473–496
30. Hanifa N, et al (2014) Interplate coupling model off the southwestern coast of Java, Indonesia, based on continuous GPS data in 2008–2010. Earth and Planetary Science Letters 401:159-171
31. Harris R, Major J (2016) Waves of destruction in the East Indies: the Wichmann catalogue of earthquakes and tsunami in the Indonesian region from 1538 to 1877. Geological Society London, Spec. Pub. 441:9–46
32. Harris R (2011) The nature of the Banda Arc–continent collision in the Timor region. In: D Brown and P Ryan (ed) Arc Continent Collision, Springer Verlag, Berlin Heidelberg, pp 163-211
33. Hébert H et al (2012) The 2006 July 17 Java (Indonesia) tsunami from satellite imagery and numerical modelling: a single or complex source? Geophysical J International 191.3:1255-1271
34. Hogg A, et al (2013) SHCal13 Southern Hemisphere calibration, 0–50,000 years cal BP. Radiocarbon 55.4:1889-1903
35. Koulali A, et al (2017) The kinematics of crustal deformation in Java from GPS observations: Implications for fault slip partitioning. Earth and Planetary Science Letters 458:69-79
36. Ishizawa T, et al (2020) Dating tsunami deposits: Present knowledge and challenges. Earth-Science Reviews 200: 102971
37. Kato Y, Akamine N, Ohori K, Tamaki T, Tamura K (1991) Movement of limestone blocks by wind waves — an example by typhoon no. 21, 1990, at Zanpa Cape, Okinawa Island, Southwestern Japan. Proceedings of Uni. Ryukyus 51:19–33
38. Kato Y, Uema K, Yamaoka N (1995) Movement of limestone-blocks by wind waves—an example by typhoon no. 13, 1994 at the south coast of Yonaguni Island, southwestern Japan. Proceedings of Univ. Ryukyus 59:29–41
39. Lau A, et al (2015) Advantages of beachrock slabs for interpreting high-energy wave transport: Evidence from Ludao Island in south-eastern Taiwan. Geomorphology 228:263-274

40. Lay T, et al (2005) The great Sumatra-Andaman earthquake of 26 December 2004. Science 308.5725:1127-1133.
41. Lorang M (2000) Predicting threshold entrainment mass for a boulder beach. J of Coastal Research. 432-445.
42. Major J, Harris R, et al (2013) Quaternary hinterland evolution of the active Banda Arc: Surface uplift and neotectonic deformation recorded by coral terraces at Kisar, Indonesia. J of Asian Earth Sciences 73:149-161.
43. Maramai A, Tinti S (1997) The 3 June 1994 Java tsunami: A post-event survey of the coastal effects. Natural Hazards 15.1:31–49
44. Mastronuzzi G, Sans`o P (2000) Boulders transport by catastrophic waves along the Ionian coast of Apulia (Southern Italy). Marine Geology 170.1-2:93–103
45. Meservy W (2017) Evaluating the East Java Tsunami Hazard: What Can Newly Discovered Imbricate Coastal Boulder Accumulations Near Pacitan and at Pantai Papuma, Indonesia Tell Us? MSc. Thesis, Brigham Young University, https://scholarsarchive.byu.edu/etd/6545
46. Milliman J (1974). Marine carbonates. Springer-Verlag, Heidelberg
47. Moore A et al (2011) Sedimentary deposits from the 17 July 2006 Western Java Tsunami, Indonesia: use of grain size analyses to assess tsunami flow depth, speed, and traction carpet characteristics. Pure and Applied Geophysics 168:1951-1961
48. Morton R, Gelfenbaum G, Jaffe BE (2007) Physical criteria for distinguishing sandy tsunami and storm deposits using modern examples. Sedimentary Geology 200.3-4:184-207
49. Mulyana A (2018) Hubungan Penyuluhan Terhadap Pengetahuan Siswa Tentang Penanggulangan Bencana Gempa Bumi Di SMK Bhakti Kencana Tasikmalaya. Jurnal Mitra Kencana Keperawatan Dan Kebidanan 1.2:1-10
50. Nandasena N, Paris R, Tanaka N (2011a) Numerical assessment of boulder transport by the 2004 Indian Ocean tsunami in Lhok Nga, West Banda Aceh (Sumatra, Indonesia). Computers & Geosciences 37.9:1391-1399
51. Nandasena N, Paris R, Tanaka N (2011b) Reassessment of hydrodynamic equations: Minimum flow velocity to initiate boulder transport by high energy events (storms, tsunamis). Marine Geology 281.1-4:70–84
52. Newcomb K, McCann W (1987) Seismic history and seismotectonics of the Sunda arc. J of Geophysical Research: Solid Earth 92.B1:421–439
53. Noormets R, Crook K, Felton E (2004) Sedimentology of rocky shorelines. Hydrodynamics of megaclast emplacement and transport on a shore platform, Oahu, Hawaii. Sedimentary Geology 172.1-2:41–65
54. Nott J (1997) Extremely high-energy wave deposits inside the Great Barrier Reef, Australia: determining the cause—tsunami or tropical cyclone. Marine Geology 141.1-4:193–207

55. Nott J (2000) Records of prehistoric tsunamis from boulder deposits: evidence from Australia. Science of Tsunami Hazards 18.1:3-14
56. Nott J (2003) Tsunami or storm waves: Determining the origin of a spectacular field of wave emplaced boulders using numerical storm surge and wave models and hydrodynamic transport equations. J of Coastal Research 4:348–356
57. Nott J (2004) The tsunami hypothesis—comparisons of the field evidence against the effects, on the western Australian coast, of some of the most powerful storms on earth. Marine Geology 208.1:1–12
58. Nott J and Bryant E (2003) Extreme marine inundations (tsunamis?) of coastal western Australia. J of Geology 111.6:691-706
59. Nugroho H, Harris R, Lestariya A, Maruf B (2009) Plate boundary reorganization in the active Banda Arc–continent collision: Insights from new GPS measurements. Tectonophysics, 479.1-2:52-65
60. O'Connor S, et al (2010) Pre-bomb marine reservoir variability in the Kimberley region, Western Australia. Radiocarbon 52.3:1158-1165
61. Oetjen J, Engel M, Schüttrump H (2021) Experiments on tsunami induced boulder transport–A review. Earth-Science Reviews 220:103714
62. Oak H (1984) The boulder beach: a fundamentally distinct sedimentary assemblage. Annals Assoc. Am. Geol., 74:71-82
63. Paris R, Wassmer P, Lavigne F, et al (2014) Coupling eruption and tsunami records: the Krakatau 1883 case study. Indonesia. Bulletin of Volcanology 76.4:1–23
64. Polet J, Thio H (2003) The 1994 Java tsunami earthquake and its “normal” aftershocks. Geophysical Research Letters 30.9
65. Pradjoko E, Kusuma T, Setyandito O, Suroso A, Harianto B (2015) The tsunami run-up assessment of 1977 Sumba Earthquake in Kuta, Center of Lombok, Indonesia. Procedia Earth and Planetary Science. 1.14:9-16
66. Prendergast A, Brown N (2012) Far-field impact and coastal sedimentation associated with the 2006 Java tsunami in West Australia. Natural Hazards 60:69-79
67. Reimer P, et al (2013) IntCal13 and Marine13 radiocarbon age calibration curves 0–50,000 years cal BP. Radiocarbon 55.4:1869-1887
68. Rizal Y, et al (2017) Tsunami evidence in south coast java, case study: Tsunami deposit along south coast of Cilacap. IOP Conference Series: Earth and Environmental Science. 71.1
69. Russell R (1963) Recent Recession of Tropical Cliffy Coasts: Elevated benches and other coastal forms give evidence of eustatic changes in sea level. Science 139.3549:9-15
70. Saintilan N, Rogers K (2005) Recent storm boulder deposits on the Beecroft Peninsula, New South Wales, Australia. Geographical Research 43.4:429–432
71. Scheffers A (2001) Tsunami boulder deposits–a strongly debated topic in paleo-tsunami research. Tsunamiites. Elsevier, 353-382

72. Scheffers A (2004) Tsunami imprints on the Leeward Netherlands Antilles (Aruba, Curaçao, Bonaire) and their relation to other coastal problems. Quaternary International 120.1:163-172
73. Scheffers A (2008) Tsunami boulder deposits. Tsunamiites. Elsevier, pp 299-317
74. Scheffers A (2021) Tsunami boulder deposits–a strongly debated topic in paleo-tsunami research. Tsunamiites. Elsevier, pp 353-382
75. Scheffers A, Kelletat D (2003) Sedimentologic and geomorphologic tsunami imprints worldwide—a review. Earth-Science Reviews 63.1-2:83-92
76. Scheffers A, Kinis S (2014) Stable imbrication and delicate/unstable settings in coastal boulder deposits: Indicators for tsunami dislocation? Quaternary International 332:73-84
77. Scheffers A, Scheffers S, Kelletat D (2005) Paleo-tsunami relics on the southern and central Antillean Island arc. J Coastal Res 21.2:263–273
78. Scheffers A, et al (2009) Wave-emplaced coarse debris and megaclasts in Ireland and Scotland: boulder transport in a high-energy littoral environment. J of Geology 117.5:553-573
79. Schneider B, et al (2019) Tsunami and storm sediments in Oman: Characterizing extreme wave deposits using terrestrial laser scanning. J Coastal Conservation 23:801-815
80. Scoffin T (1993) The geological effects of hurricanes on coral reefs and the interpretation of storm deposits. Coral Reefs 12:203-221
81. Southon J, et al (2002) Marine reservoir corrections for the Indian Ocean and Southeast Asia. Radiocarbon 44.1:167-180
82. Suárez G, Albini P (2009) Evidence for great tsunamigenic earthquakes (M 8.6) along the Mexican subduction zone. B Seismological Society America 99.2A: 892-896.
83. Suanez S, Fichaut B, Magne R (2009) Cliff-top storm deposits on Banneg Island, Brittany, France: effects of giant waves in the eastern Atlantic Ocean. Sedimentary Geology 220.1-2:12–28
84. Sulaeman H (2018) Discovery of paleotsunami deposits along the eastern Sunda Arc: potential for megathrust earthquakes in Bali, MSc. Thesis, Brigham Young University, https://scholarsarchive.byu.edu/etd/
85. Switzer A, Jones B (2008) Large-scale washover sedimentation in a freshwater lagoon from the southeast Australian coast: sea-level change, tsunami or exceptionally large storm? The Holocene 18.5:787-803
86. Synolakis C, Imamura F, Tsuji Y, et al (1995) Damage, conditions of East Java tsunami of 1994 analyzed. EOS, Transactions American Geophysical Union 76.26:257–257
87. Szczucinski W (2012) The post-depositional changes of the onshore 2004 tsunami deposits on the Andaman Sea coast of Thailand. Natural Hazards 60:115–133.
88. Titov V, Kˆanoˇglu U, Synolakis C (2016) Development of MOST for real-time tsunami forecasting. PhD thesis, American Society of Civil Engineers.
89. Titov V, Moore C, Greenslade D, et al (2011) A new tool for inundation modeling: Community modeling interface for tsunamis (commit). Pure and Applied Geophysics 168.11:2121–2131

90. Tsuboi S (2000) Application of mwp to tsunami earthquake. Geophysical Research Letters 27.19:3105–3108
91. Tsuji Y, Imamura F, Matsutomi H, et al (1995a) Field survey of the east java earthquake and tsunami of June 3, 1994. In: Tsunamis: 1992–1994, Springer, pp 839–854
92. Tsuji Y, et al (1995b) Field survey of the East Java earthquake and tsunami of June 3, 1994. Tsunamis: 1992–1994: Their Generation, Dynamics, and Hazard, pp 839-854
93. Vieira M, Fernando De Ros L, Bezerra F (2007) Lithofaciology and palaeoenvironmental analysis of Holocene beachrocks in northeastern Brazil. J Coastal Research 23.6:1535-1548.
94. Vousdoukas, M, Velegrakis A, Plomaritis, T (2007) Beachrock occurrence, characteristics, formation mechanisms and impacts. Earth-Science Rev. 85.1-2:23-46
95. Wichmann A (1918) Die Erdbeben des indischen Archipels bis zum Jahre 1857, vol 20. Koninklijke Akademie van Wetenschappen, Amsterdam
96. Wichmann A (1922) Die Erdbeben des Indischen Archipels von 1858 bis 1877. Koninklijke Akademie van Wetenschappen, Amsterdam
97. Windupranata W, et al (2019) Impact analysis of Tropical Cyclone Cempaka-Dahlia on wave heights in Indonesian waters from numerical model and altimetry satellite. KnE Engineering 203-214
98. Xia Y, et al (2021) Marine forearc structure of eastern Java and its role in the 1994 Java tsunami earthquake. Solid Earth 12.11:2467-2477

# Figures

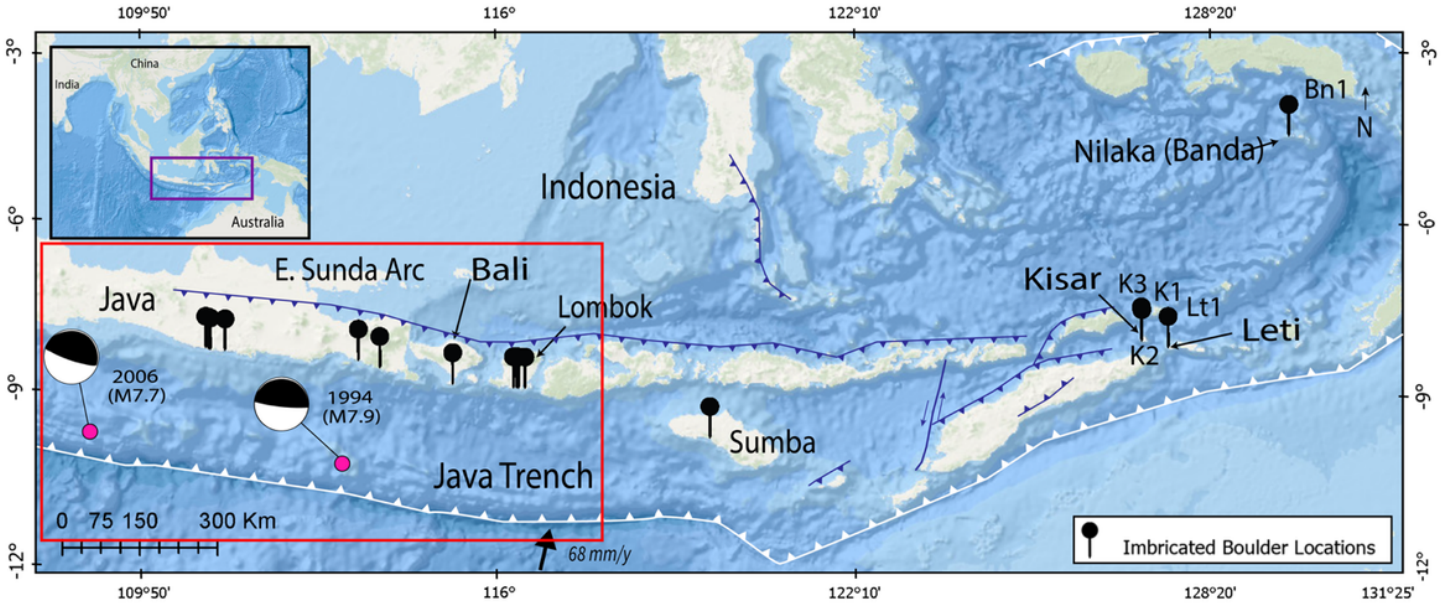


**Figure 1**

Top - Location map of eastern Sunda Arc islands, tectonic features, and all the IBD sites we investigated (black pins with site numbers). Red box is approximate location of detailed map with site numbers for Java, Bali and Lombok (Fig 2). Fault plane solutions are for the only instrumental earthquakes on the Java Trench subduction zone interface.

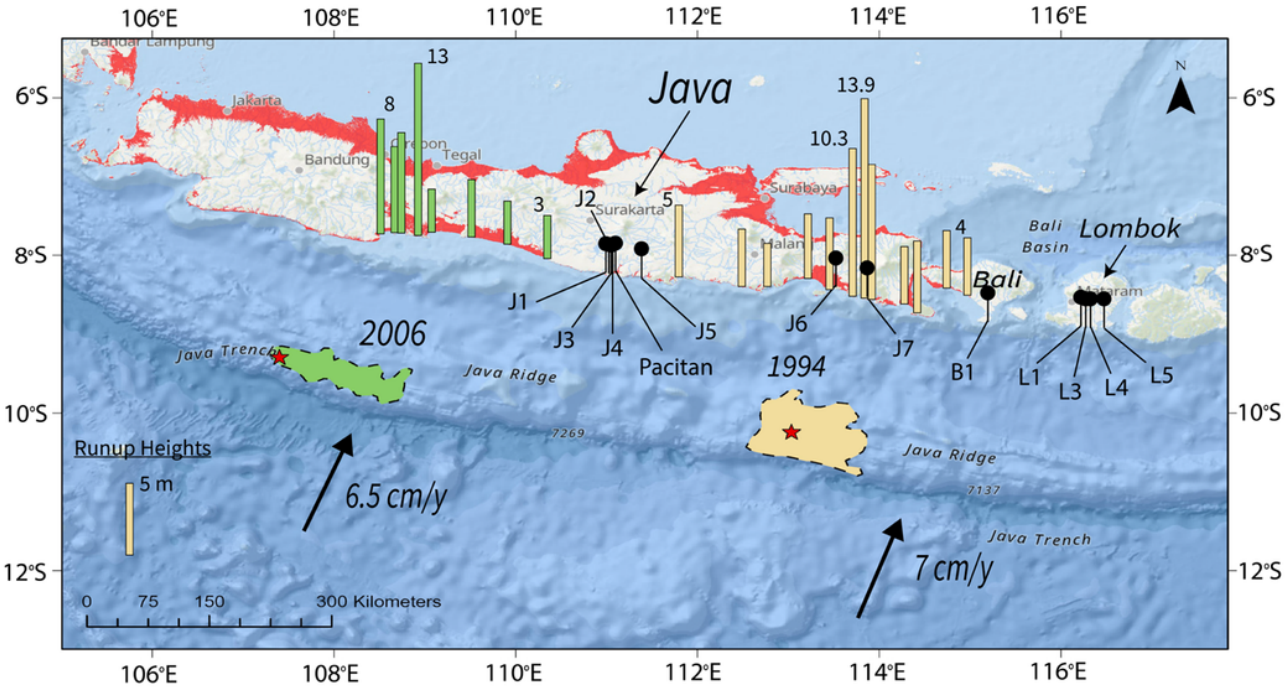


## Figure 2

Detail of IBD site locations in Java, Bali, and Lombok (black pins with site numbers). Green and tan patches are subduction interface rupture zones of the 2006 and 1994 earthquakes, respectively. Bars are run up heights of tsunamis caused by the earthquakes. The red area is < 30 m above sea level. Black arrows are plate convergence vectors.

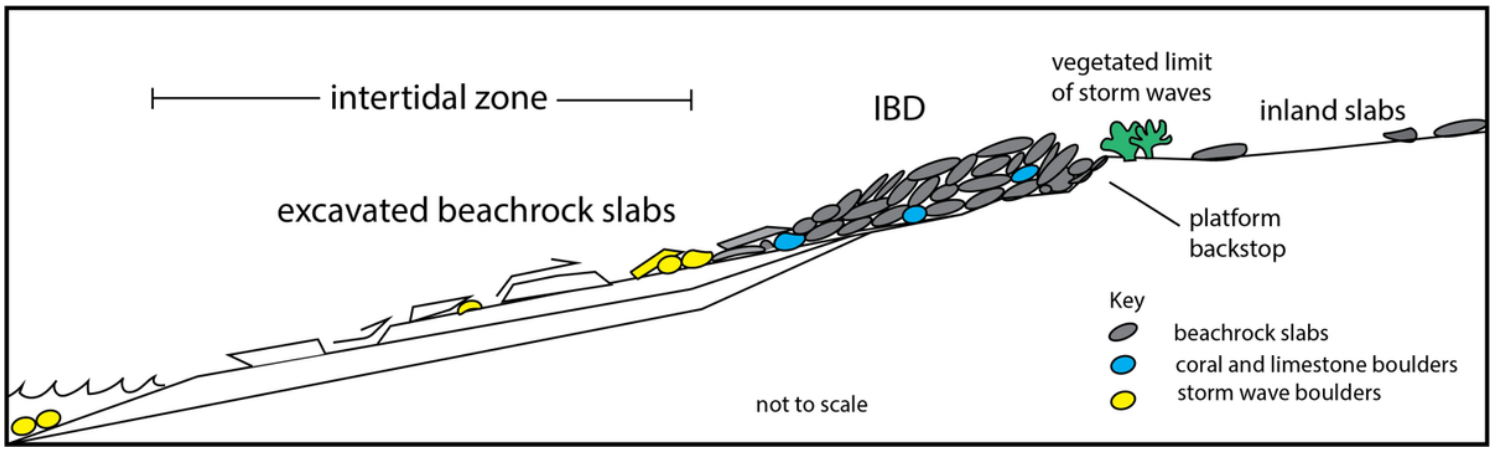


## Figure 3

Sketch of erosional and depositional settings of IBD in Indonesia. Layered beachrock (white) is torn from intertidal outcrops and stack up as imbricated slabs (grey) against a wave cut step or backstop at the rear of the supra-tidal platform. Blue – coral boulders used for age constraints. Yellow – bedrock boulders deposited by storm waves. The view is parallel to the a-axis of imbricated beachrock slabs.


## Figure 4

IBD along the southern coastlines of eastern Sunda Arc islands of Java and Lombok. (a) Looking west at Pantai Papuma (site J6, Fig 2), which was observed to form during the 1994 East Java earthquake-

generated tsunami. Notice the uniformity of imbricated beachrock slab composition, shape, and size. Deposit is stacked against landward edge of platform (see Fig 3). (b) Pantai Pedenombo (site J4) looking east. IBD forms landward of heavily solution weathered limestone ridge of the supratidal platform. Some beachrock and limestone slabs are found landward of the backstop on the forested coastal plain. Ground target for UAV is 1.2 m wide. (c) Detail of 'b' looking west. Note how IBD have different amounts of weathering and smoothness. Deposit is littered with small (<0.5m a-axis), rounded, and circular boulders we observed being deposited by wind waves (see Fig 3). Digital surface models of Pedenombo were constructed and compared to quantify storm wave influences over a 3-year period (see below). (d) UAV image of Pantai Kura-Kura (site L4) oriented east towards top. Note excavation scarps, and large, detached beachrock slabs that have not been added to the IBD yet. (e) Detail of (d) taken from western-most ground control target showing large beachrock slabs at toe of IBD.

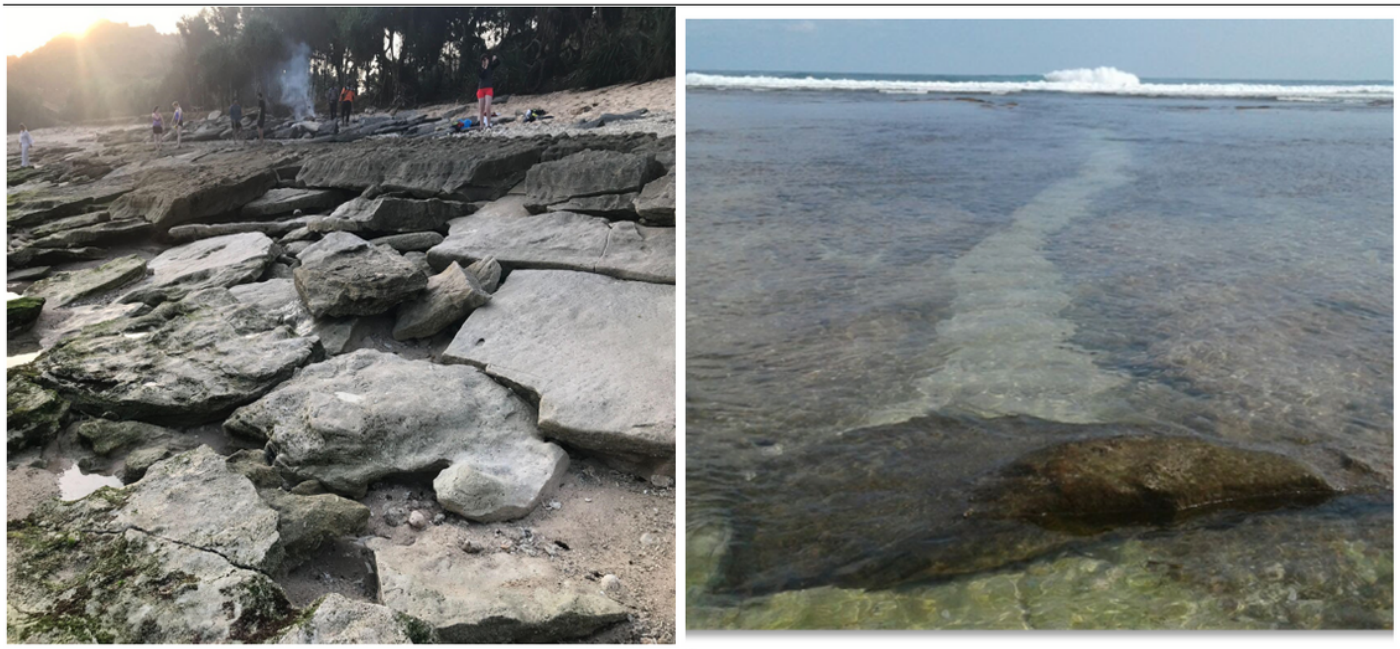


**Figure 5**

a) Beachrock slab excavation zone at Pantai Blosok (site J3). Excavation geometries have seaward dipping fault ramps and flats (see Fig. 3) where layered slabs were dislodged and transported landward against gravity. This excavation zone is typical of each IBD we discovered. Waves at Pantai Blosok normally break >200 m offshore and are said by locals to never pass beyond the mangrove trees just landward of the boulders even during high wave events. b) Looking south at coral boulder (2 x 1 x 0.4 m) in subtidal zone that was dislodged likely from the toe of the seaward platform edge and based on its distinct track, moved around 70 m toward Pantai Blosok. Notice waves breaking offshore at platform edge.

## Figure 6

Beachrock consisting of carbonate-cemented clastic and bioclastic material.

## Figure 7

Looking NW at large (~75 metric tons) imbricate boulder of volcanic rock in the intertidal zone at Payung, Lombok.

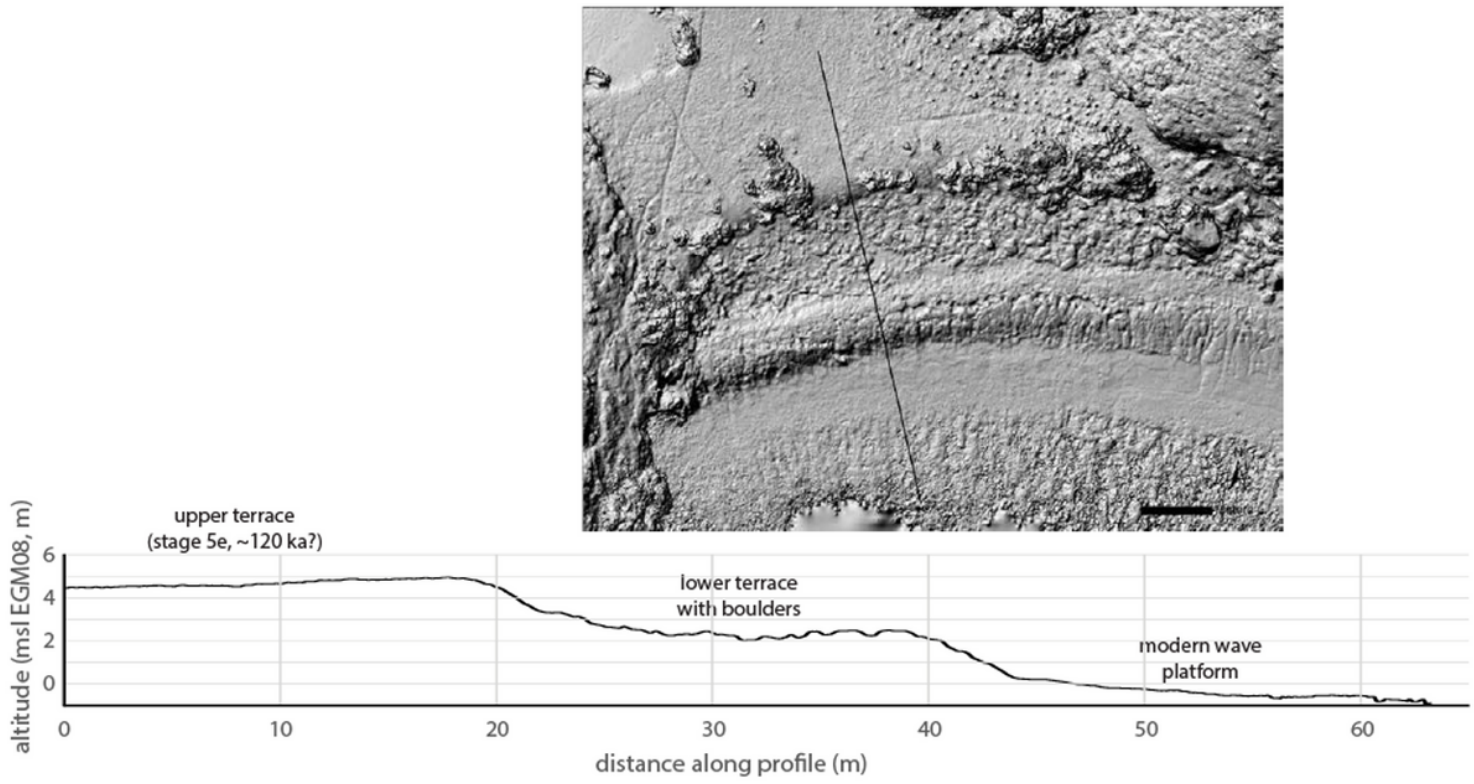


## Figure 8

Shaded relief image and profile of Pedenombo beach showing its three different platforms.

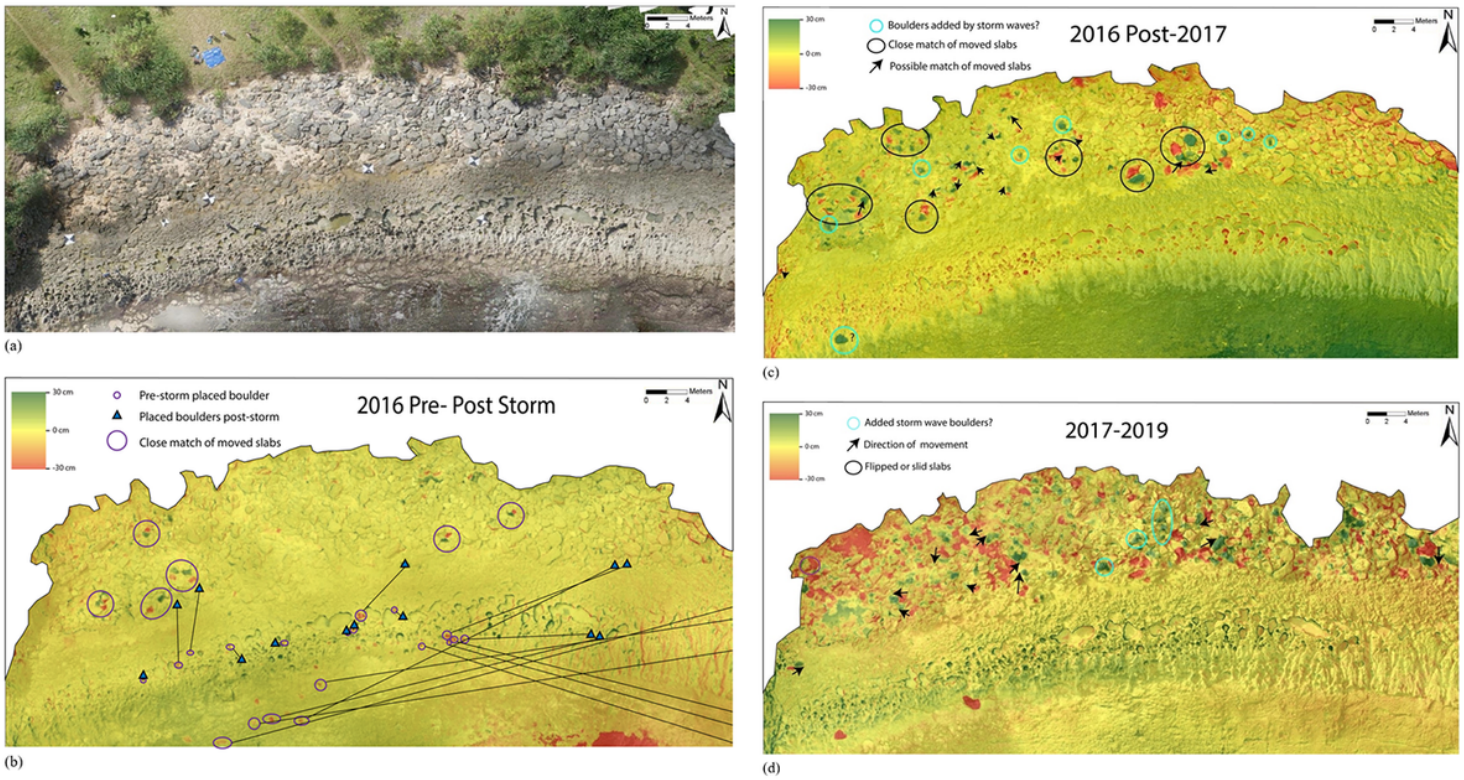


## Figure 9

**a-d** UAV generated DSM overlays taken at 4 different times over a 3-year period at Pedenombo (site J4). Red signifies negative change in elevation of < -0.3 m. Green shows an elevation increase of < +0.3 m. The outer rim of the beach shown in (a) is cropped in this and other images. Solution weathered pockets eroded into bare-rock platform 2 (Fig 8) are useful for registering images. When measuring possible beachrock slab movement over longer periods of time, correlating slab excavation and addition marks is difficult due to deposition and removal of storm wave transported sand, gravel, and cobbles.

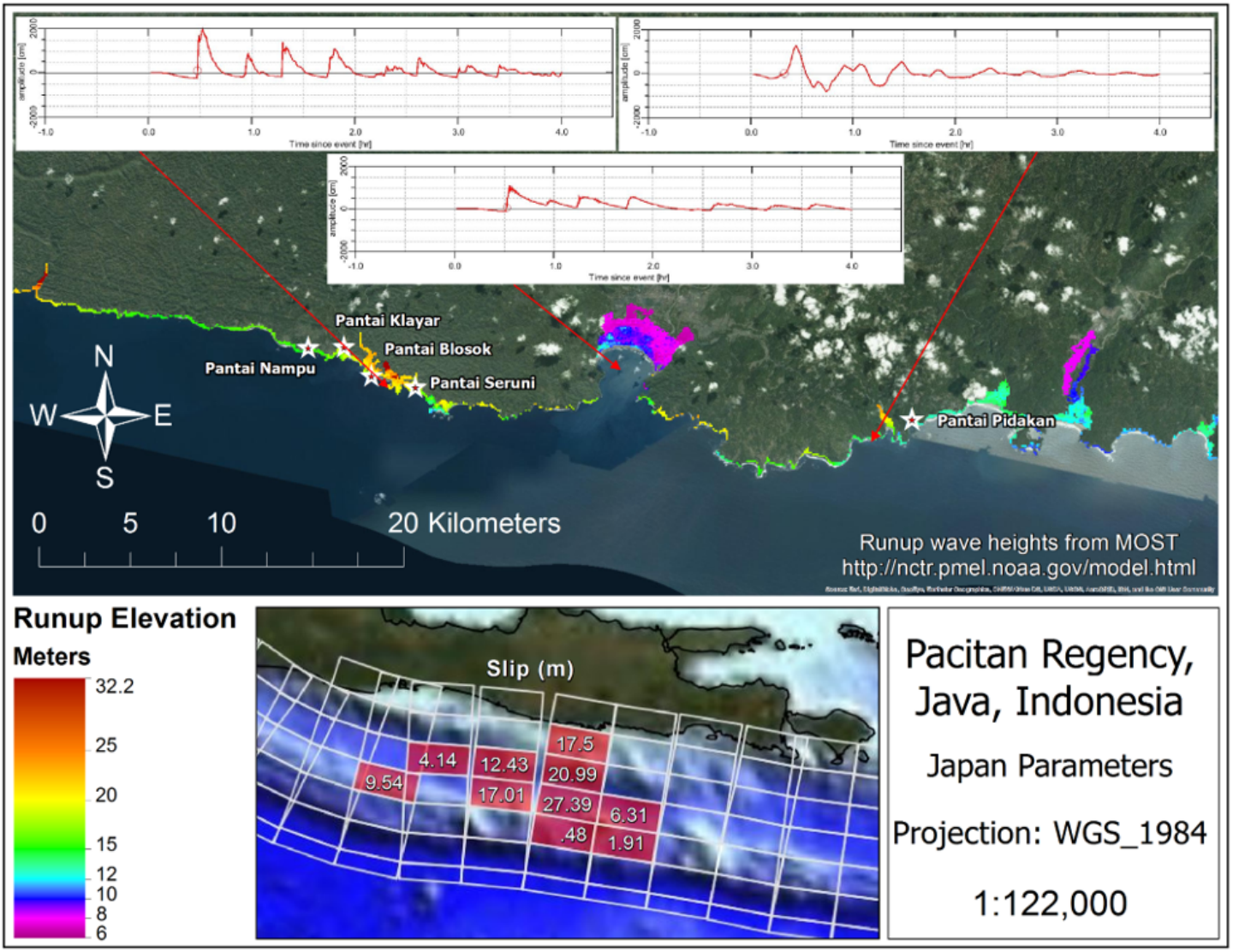


## Figure 10

Model 1 of an 8.4 Mw earthquake on the segment of the Java Trench between the locations of the 1994 and 2006 Java Trench earthquakes. The slip distribution along the fault is like that used in Titov et al. (2016) for the 2011 Tohoku earthquake. Red dots are the locations of simulated tidal gauges that match with the red lines time series data. These data predict the arrival of a ~20 m wave 20-30 minutes after the initiation of the earthquake. Interestingly, the location of the IBD (stars) is where the model predicts the highest wave runup.

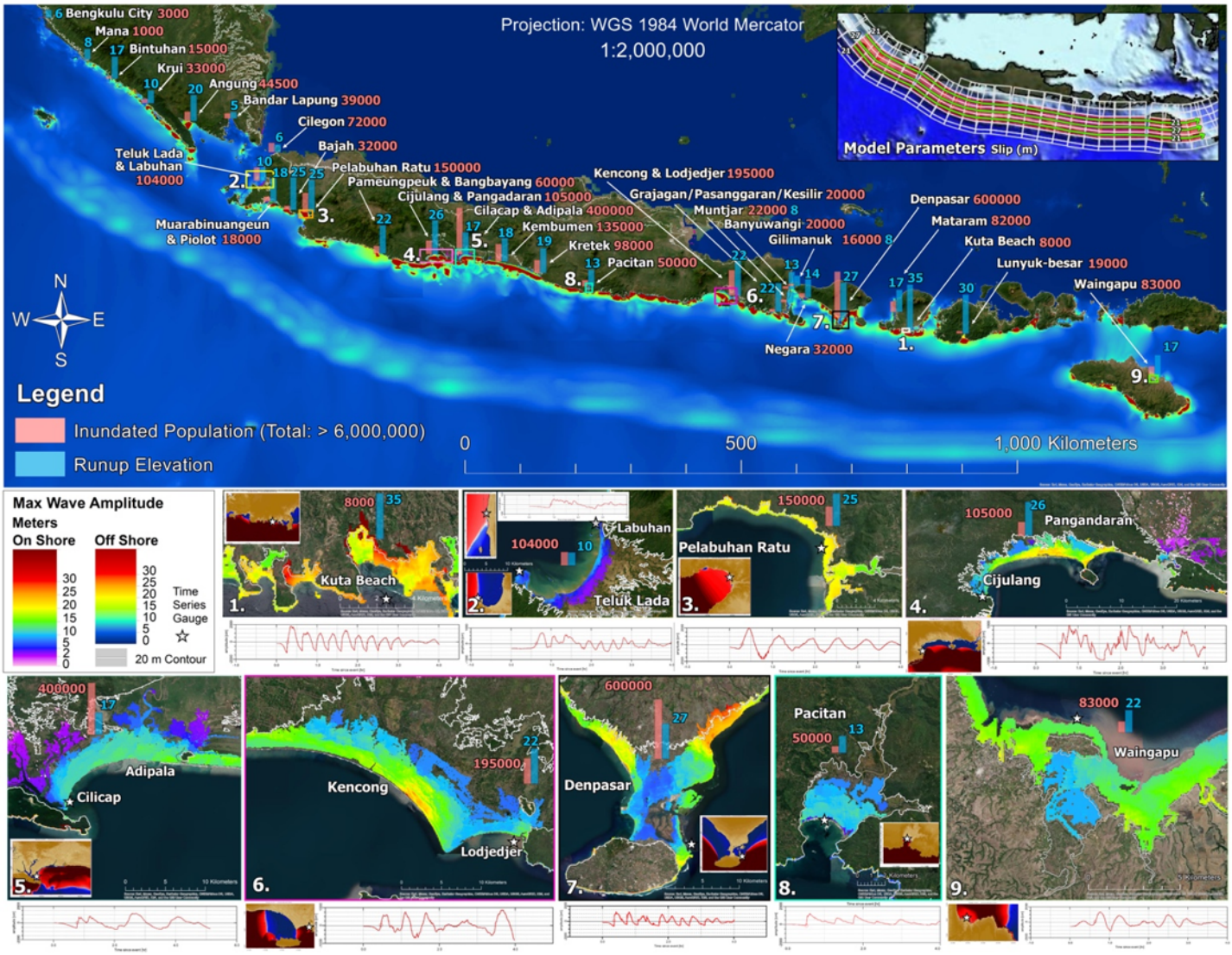


## Figure 11

Model 2 of full Java Trench seismic gap rupture (from southern-most Sumatra to Sumba). Model slip distribution is shown in upper right. Top map shows inundation, runup (blue bar) and population estimates of cities in the inundation zone (red bar). The total number of inhabitants living in the inundation zone is around 6 million. Bottom - detailed maps of the most populated areas. Small inset map shows arrival of first wave offshore next to four-hour time series of wave arrivals. The grey line onshore is the 20 m elevation contour.

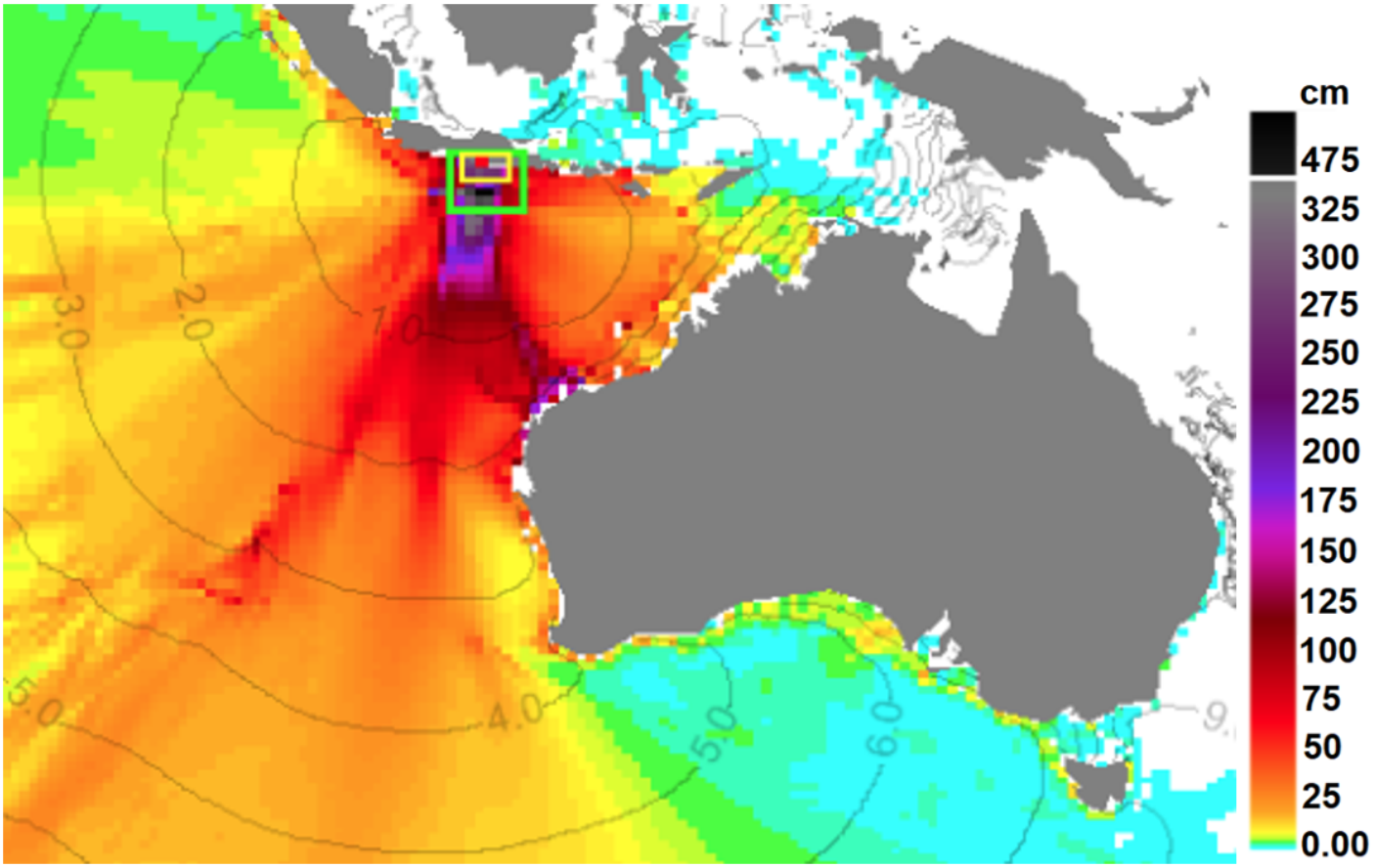


**Figure 12**

Model 2 trans-oceanic wave height distribution showing tendrils of highest waves (dark colors) focusing energy on the Exmouth, Australian region where IBD are observed.